Galileo Ultraviolet Spectrometer Observations of Jupiter's Auroral Spectrum from 1600-3200 Å

Wayne R. Pryor[1], Joseph M. Ajello[2], W. Kent Tobiska[3], Donald E. Shemansky[4], Geoffrey K. James[2], Charles W. Hord[1], Stuart K. Stephens[3], Robert A. West[2], A. Ian F. Stewart[1], William E. McClintock[1], Karen E. Simmons[1], Amanda R. Hendrix[1], Deborah A. Miller[1]

[1]Laboratory for Atmospheric and Space Physics, 1234 Innovation Drive, University of Colorado, Boulder, CO 80303

[2]Jet Propulsion Laboratory, MS 183-601, 4800 Oak Grove Drive, Pasadena, CA 91109

[3]FDC/Jet Propulsion Laboratory, MS 264-580, 4800 Oak Grove Drive, Pasadena, CA 91109

[4]University of Southern California, Dept. of Aerospace Engineering, Los Angeles, CA 90089

As revised for JGR 3/4/98

Galileo ultraviolet spectrometer observations of Jupiter's auroral spectrum from 1600-3200 Å

Wayne R. Pryor,[1] Joseph M. Ajello,[2] W. Kent Tobiska,[3] Donald E. Shemansky,[4] Geoffrey K. James,[2] Charles W. Hord,[1] Stuart K. Stephens,[3] Robert A. West,[2] A. Ian F. Stewart,[1] William E. McClintock,[1] Karen E. Simmons,[1] Amanda R. Hendrix,[1] and Deborah A. Miller[1]

Abstract. In 1996 and 1997 the Galileo Ultraviolet Spectrometer (UVS) obtained the first measurements of Jupiter's nightside midultraviolet (MUV) polar auroral spectrum from 1620 to 3231 Å at 13 Å resolution. The reduced polar spectra, after removal of off-axis scattered radiation from the sunlit dayside of Jupiter, contain a spectrum that matches laboratory spectra of the H_2 continuum in the *a-b* dissociative emission transition. This is the first direct identification of the H_2 *a-b* transition in astronomy. The *a-b* emission is excited by electron impact exchange reactions with H_2 that peak in cross section near 15 eV. The emission threshold is at 1216 Å, and the continuum peaks in intensity in the 2000-2500 Å range. Jupiter's observed wavelength-integrated MUV H_2 *a-b* emissions (1620-3231 Å) have a photon flux ~8 times smaller than simultaneously observed wavelength-integrated far-ultraviolet (FUV) H_2 band emissions (1230-1650 Å). Because the FUV H_2 emissions have an emission cross section that peaks at higher energies near 50 eV, this FUV/MUV brightness ratio is diagnostic of the secondary electron energy distribution and is consistent with a "warm" distribution of electrons.

1. Introduction

Jupiter's aurora has been extensively studied with sounding rockets, spacecraft, and ground-based telescopes in the X ray, extreme ultraviolet (EUV), FUV, and infrared (see the review by *Ajello et al.* 1998, [this issue]). Part of the energy deposited by particle precipitation is reemitted in photons produced in transitions in H, H_2, CH_4, C_2H_2, C_2H_6, H_3^+, and other gases. Emissions in the 500-1200 Å EUV and 1200-1700 Å FUV spectral regions are due to electron and ion impact excitation of H_2 and H. Recent Galileo ultraviolet spectrometer (UVS) FUV Jupiter auroral spectra are remarkably similar to nearly simultaneous low-resolution Jupiter FUV auroral spectra obtained by J. Clarke with the Goddard high resolution spectrograph on the Hubble Space Telescope (HST) [*Ajello et al.*, this issue]. Galileo EUV and FUV auroral spectra are different from an optically thin laboratory spectrum of electrons bombarding H_2 because of self-absorption effects in H_2 gas, absorption in CH_4 (methane) and C_2H_2 (acetylene), and absorption from larger hydrocarbons and from aerosols [*Ajello et al.*, this issue]. Away from the auroral regions, the poles are quite dark in the HST Wide Field Planetary Camera 2 (WFPC-2) FUV images that have some sensitivity to the MUV [*Clarke et al.*, 1996]. The hydrocarbons and aerosols that darken the FUV polar images and modify the auroral spectra are probably produced from methane by the polar auroras. The auroras contain more energy for methane dissociation than is available in sunlight for methane Lyman α photolysis in the polar regions [*Hord et al.*, 1979; *Pryor and Hord*, 1991].

The MUV auroral spectrum from 1700-3200 Å was previously unexplored because reflected sunlight from Jupiter's atmosphere overwhelms the auroral emissions as seen from the vicinity of Earth. This is not true in the EUV and FUV because

the solar flux is several orders of magnitude weaker than in the MUV and because the H_2 emissions are brightest in the EUV and FUV. Galileo's unique ability to observe Jupiter's darkside has now produced the first MUV auroral spectra. This paper describes two types of MUV darkside spectra.

1. Darkside spectra of Jupiter obtained near 90° phase angle that contain off-axis scattered radiation from Jupiter's dayside, but could be obtained with a long integration period to obtain reasonable signal-to-noise.

2. Darkside spectra of Jupiter's southern aurora obtained from within the shadow of Jupiter that contain less off-axis scattered radiation from the dayside, but have low signal-to-noise.

As we will show, the 90° phase angle MUV polar auroral spectra from the nightside have a distinct wavelength-dependent emission that is not due to off-axis scattered radiation from the dayside. The MUV auroral spectrum is consistent with laboratory measurements of the H_2 *a-b* continuum radiation obtained by *James et al.* [this issue] in electron impact experiments. Simultaneous FUV/MUV spectra obtained within Jupiter's shadow clearly show bright FUV aurora but proved inconclusive in the MUV due to short integration times and a low signal-to-noise ratio.

2. Instrumentation

The Galileo UVS instrument [*Hord et al.*, 1992] consists of a Cassegrain telescope and a Fastie-Ebert spectrometer. The spectrometer uses a scanning grating drive to obtain spectra with three different photomultiplier tubes. FUV spectra are measured with a "G" tube with a CsI photocathode in second order from 1133 to 1921 Å at 6.7 Å resolution. MUV spectra are measured from 1620 to 3231 Å with 13.6 Å resolution in first order using an "F" tube with a CsTe photocathode. Near-ultraviolet (NUV) spectra from 2820 to 4320 Å are measured with 13.6 Å resolution in first order using an "N" tube with a KCsSb photocathode. The G and N slits have the same field of view, measuring 0.1 by 1.0° on the sky. The F slit used for the MUV spectra described here is shorter in one dimension, measuring 0.1 by 0.4°. The centers of all three slits are boresighted, that is, they all look in the same direction. It requires 4 1/3 s to obtain an F-channel or G-channel spectrum, including a 1/3 s dead time for large grating motions and a 4 s interval in which smaller grating steps occur 528 times 7.57 ms apart. Actual data integration lasts 6 ms on each 7.57 ms step. Each F channel step is spectrally displaced by 3.1 Å, and samples light from a range of wavelengths 13.6 Å wide full-width at half maximum (FWHM). The F-channel recorded counts for each step are always log-compressed into 8-bit numbers by the UVS electronics. We have adopted the in-flight stellar calibration of the F-channel described by *Hendrix* [1996].

The data collection system can be configured into two modes. The recorded mode was used for observations obtained with Galileo inside Jupiter's shadow. In recorded mode each 8-bit element of data is stored separately for eventual transmission to Earth, allowing accurate reconstruction of the uncompressed tube counts at low count rates. Recorded mode is re-

A data record is one readout (flush) of the spacecraft RTS data buffer containing (in our MUV RTS data sets) a single F and a single G summed spectrum.

The geometry of the auroral ovals is not symmetric between north and south; the northern oval contains the most equatorward segment of the auroral arcs, near longitude 180°. Thus the maximum angular distance of the northern oval from the north pole viewed from Galileo is larger than the maximum angular distance of the southern oval from the south pole. This implies that the most favorable MUV observations may come from the north, when 180° is near the dark limb, providing the largest angle between the terminator and the auroral emissions in order to minimize off-axis light. Figure 1b illustrates the observing geometry for a typical darkside observation near 90° phase angle.

3.2. Observations From Within Jupiter's Shadow

On 1996 day 314 during the "Callisto 3" (C3) orbit, the Galileo spacecraft was turned to observe Jupiter's darkside from within Jupiter's shadow. UVS-recorded observations were obtained for 66 m 44 s during this turn, although only half of this was returned due to downlink limitations. The UVS observing strategy selected for the south polar observations involved alternating 4 1/3 s spectral scans of the F (MUV) and G (FUV) tubes, of which 12 m 8 s were returned. Figure 2 shows the observing geometry for the south polar observations. The F-channel slit observed darkside emissions from 100-130° System III longitude. The FUV and MUV total counts per spectrum as a function of time are shown in Figure 3. The FUV count rates peak when the slit was near the central meridian on the darkside, due to auroral emissions. The MUV count rates peak at the beginning of the observation, when the slit was pointed at the planetary limb. Figure 4 shows the summed FUV and MUV spectra for this period. The FUV spectrum shows the usual H_2 band emission pattern seen in UVS lab spectra of electron impact on H_2 [*Hord et al.*, 1992] and UVS Jupiter spectra [*Ajello et al.*, this issue]. The MUV spectrum agrees well with a least squares fit spectrum formed from a solar spectrum [*Van Hoosier et al.*, 1988] multiplied by the instrument calibration. We conclude that the MUV spectrum seen here is due to forward-scattered sunlight. A similar fit is obtained if a dayside Jupiter spectrum from UVS is used instead of a solar spectrum. Because the G slit is longer than the F slit, it is possible that the observed FUV emissions originated outside the field of view of the F slit. This low signal-to-noise data set is consistent with the absence of an MUV aurora and shows that any MUV aurora is considerably weaker than the FUV aurora.

Fig 2

Fig 3

Fig 4

Better MUV auroral observations were obtained at 90° phase that allow us to quantify the FUV/MUV brightness ratio. North polar observations during the C3 turn obtained by alternating the N (NUV) and G channels did not detect auroral emissions in either channel, confirming that the northern auroral oval was not in the field of view due to a late trajectory update. Additional NUV darkside observations from within Jupiter's shadow were obtained on orbit C10.

3.3. Laboratory Spectra

We now describe the process of separating the nightside auroral spectrum from the somewhat brighter off-axis scattered radiation from Jupiter's dayside. Inspection of the data set suggests that darkside spectra are generally similar to the dayside reflected light spectra, but the darkest darkside polar spectra have a somewhat different spectral appearance, suggesting the presence of an auroral component. To improve the signal-to-noise ratio, we summed darkside polar observations that had relatively small radiation background and off-axis scattered radiation signatures. Figure 5 shows the sum of the north and south polar darkside MUV spectra obtained near 90° phase to date, with the selection criterion that the count rate in channel 420 at 2910 Å, near the peak of the Jupiter dayside spectrum, was below 50 counts/s. Nine records of data met this criteria and are so marked in Table 1. This summed spectrum has a spectral wavelength dependence with relatively more emission at wavelengths below 2800 Å than does the dayside spectrum. We examined multiple linear regression [*Bevington*, 1969] models of this spectrum involving various regression components that included a wavelength-independent background, a reference dayside spectrum, and laboratory electron impact spectra. First, we fit the summed spectrum with only a reference dayside spectrum, where the solar reflected light is dominant and has high signal-to-noise. This regression in the software package Interactive Data Language (IDL) produces a "reduced and weighted" χ^2 of 1.13, but is a fairly poor fit, with this model larger than the data at the shortest wavelengths and smaller than the data in the wavelengths near 2300 Å where H_2 emission is expected to be visible. If the fitting function is a good approximation to the parent function, then the value of the reduced χ^2 should be approximately 1. Next, we tried a regression involving both the reference dayside spectrum and a calibrated 14 eV laboratory spectrum (multiplied by the UVS response curve). This model produces a visually appealing fit throughout the spectrum with a reduced χ^2 of 1.02. A regression with both the reference dayside spectrum and a 19 eV laboratory spectrum (multiplied by the UVS response curve) produces a somewhat worse fit, with a reduced χ^2 of 1.06. The 14 eV and 19 eV laboratory spectra are sufficiently similar that the regression program by itself could not meaningfully assess their relative contributions. Figure 6 shows the summed darkside spectrum after subtraction of (1) the solar component when the 14 eV spectrum was the other component in the regression and (2) the solar component when the 19 eV spectrum was the other component. The nonsolar component of the darkside spectrum strongly resembles the 14 and 19 eV laboratory spectra, with a somewhat better match for the 14 eV spectrum.

Fig 5

Fig 6

Examination of a summed darkside equatorial MUV spectrum (Figure 7) reveals no obvious pattern other than the off-axis dayside spectrum. The same reference reflected solar spectrum fits this spectrum with a reduced χ^2 of 1.17. In this case, adding the 14 eV or 19 eV components to the regression did not change the quality of fit χ^2 significantly: the new fits also have χ^2 of 1.17. We interpret the lack of a 14 eV or 19 eV component in the equatorial spectrum as further evidence that the high-latitude deviation in the MUV spectrum from the off-axis dayside spectrum is a phenomenon caused by the polar

Fig 7

occurring by chance when the number of degrees of freedom is large. We conclude that the additional term, the 14 eV H_2 *a-b* laboratory spectrum, is significant.

5. MUV and FUV Brightnesses

The near 90° phase angle data were used to find the relative brightness of the FUV and MUV auroras. Figure 8 shows the summed FUV polar spectrum obtained simultaneously with the summed MUV polar spectrum of Figure 5. This FUV polar spectrum is similar to a 100 eV e^- on H_2 FUV spectrum obtained with the UVS in the laboratory [*Ajello et al.* 1988]. Below about 1400 Å, the spectra differ due to methane absorption from gas located above the auroral emissions and due to differences in the electron energy distribution [*Ajello et al.*, this issue]. Deliberately excluding Lyman α, we find the total number of G-channel (FUV) counts between 1230 and 1650 Å (after background subtraction) is 40,839. The total number of F-channel (MUV) counts (after subtracting a wavelength-independent background and the off-axis dayside scattered radiation contribution) is 5836. To estimate the relative emission rates requires some assumptions, because the G-channel slit is longer than the F-channel slit. If the two fields of view are filled, the wavelength-integrated signal in the G-channel (here restricted to 1230-1650 Å) is 5.8 kiloRayleighs (kR), and in the F-channel (1616.5-3227.9 Å) is 1.8 kR. In reality, the auroral arc is probably quite narrow (~200 km) in width and fills a small fraction of each slit. The actual G-channel/F-channel brightness ratio in the arc is better approximated by (5.8/1.8)(1.0°/0.4°)=8.1, where 1.0° and 0.4° are estimates for the effective slit lengths of the G and F channels, respectively. This correction is invalid if part of the emission occurs in portions of the G-channel slit that extend beyond the region of overlap with the F-channel slit. In the calibrated 14 eV e^- on H_2 laboratory spectrum the brightness ratio between G-channel (1230-1700 Å) and F-channel (1616.5-3227.9 Å) wavelengths is 1.3, at 19 eV the ratio is 2.25, and at 100 eV the ratio is 9.9. The ratio at 100 eV is lower than that expected from the (*a-b*) model of *Ajello and Shemansky* [1993]. The unexpectedly strong H_2 (*a-b*) spectrum at 100 eV can be explained by (1) a large number of low energy secondary electrons trapped in the collimating magnetic field that efficiently excite the continuum or/and (2) a very strong cascade channel from the many upper-lying triplet states that contains a large singlet-triplet mixing. The arc-width estimate of 200 km comes from imaging of the spatially resolved arc by the Galileo solid state imager (SSI) in visible and near-infrared wavelengths (A. Ingersoll et al., Imaging Jupiter's aurora at visible wavelengths, submitted to *Journal of Geophysical Research*, 1998). The F-channel region from 1616.5 to 3227.9 Å comprises ~75% of the photons emitted in the whole H_2 (*a-b*) system (1216-∞ Å) if the spectrum is due to 14 eV electrons striking H_2.

The measured ratio of FUV/MUV brightness can be compared to theoretical expectations. The secondary electron energy distribution measured in the laboratory increases at lower energies and can be represented as a sum of 4 Maxwellians [*Opal et al.*, 1971; *Ajello et al.*, this issue]. In *Ajello et al.'s*

6. Discussion

To the best of our knowledge, Galileo UVS has provided the first spectral observation of the H_2 *a-b* continuum emission in any astrophysical object. The H_2 *a-b* band system may be an important process for (1) heating outer planet atmospheres, molecular clouds in the interstellar medium, and stellar atmospheres of cool stars and (2) measuring the secondary electron energies. Fast atomic hydrogen H(1*s*) atoms made in the *a-b* transition with characteristic energies of 3 eV (23,000 K) will heat Jupiter's atmosphere through collisions. Diagnosing the secondary electron spectrum is also of importance because the secondaries are responsible for most of the emissions [*Rego et al.*, 1994]. It is not too surprising that the MUV auroral spectrum resembles that of H_2 excitation by electrons with 14 eV impact energy. H_2 is the most abundant gas in the Jupiter atmosphere. The manifold of triplet states of H_2 has large excitation cross sections for the *a, b, c, d, e* states in the threshold region near 15 eV [*Ajello and Shemansky*, 1993; *Khakoo and Trajmar*, 1986]. The triplet states (*c, d, e,...*) with higher excitation energy than the *a* state relax by dipole allowed radiative transitions to the *a* state, followed by an allowed transition to the *b* state. MUV spectral data are sensitive to electron energies near 15.5 eV, the peak in the *a-b* emission cross section. Simultaneously modeling the FUV and MUV brightnesses has provided an important test of the secondary electron distribution, with the surprising result that a warm electron distribution with energies near 27 eV is consistent with the brightness ratio.

The Galileo UVS Jupiter MUV spectra agree with the laboratory data on electron impact on H_2 quite well. However, in the FUV, substantial hydrocarbon absorptions modify the auroral spectrum substantially [*Ajello et al.*, this issue]. Reflection from below may also be important. *Yung et al.* [1982] estimated that a ~20% enhancement of the FUV Lyman bands occurs due to reflection of downward flux by Rayleigh scattering of H_2. We now consider possible corrections for MUV absorptions and reflections. The reflected sunlight spectrum of Jupiter in the MUV was measured by the International Ultraviolet Explorer (IUE) [*Wagener et al.*, 1985] and by Galileo UVS [*Hord et al.*, 1995]. At Galileo UVS resolution, the reflected sunlight spectrum is modified by the presence of aerosols, but no characteristic absorptions can be resolved. At IUE resolution, NH_3 bands are seen [*Wagener et al.*, 1985]. However, ammonia absorption occurs below the NH_3 cloud layer at the several hundred millibar level; this is well below the auroral emissions at pressures near the microbar level. Hydrocarbon and aerosol absorptions remain possible in the auroral spectrum, but based on the Galileo reflected sunlight spectrum we expect to see nearly grey continuum absorption. *Wagener et al.* [1985] modeled the IUE equatorial MUV continuum absorption from 2400 to 3200 Å with two haze layers: a 1.5 optical depth haze homogeneously distributed from 150 to 600 millibar with a constant single-scattering albedo of 0.42; and a high (50 millibar), thin (0.25 optical depth) haze of single-scattering albedo 0.97. *Wagener and Caldwell* [1988] next examined the latitude dependence of the continuum absorption in IUE spectra and found the upper haze occurs higher in the polar atmosphere, somewhere in the 0-50 millibar region. These

References

Ajello, J. M., and D. E. Shemansky, Electron excitation of the $H_2(a\ ^3\Sigma_g^+ \rightarrow b\ ^3\Sigma_u^+)$ continuum in the vacuum ultraviolet, *Astrophys. J., 407*, 820-825, 1993.

Ajello, J. M., et al., Simple ultraviolet calibration source with reference spectra and its use with the Galileo orbiter ultraviolet spectrometer, *Appl. Opt., 27*, 890-914, 1988.

Ajello, J. M., G. K. James, B. O. Franklin, and D. E. Shemansky, Medium-resolution studies of extreme ultraviolet emission from N_2 by electron impact: Vibrational perturbations and cross sections of the $c_4'\ ^1\Sigma_u^+$ and $b'\ ^1\Sigma_u^+$ states, *Phys. Rev. A, 40*, 3524-3556, 1989.

Ajello, J. M., et al., Galileo orbiter ultraviolet observations of Jupiter aurora, *J. Geophys. Res.*, this issue.

Belton, M. J. S., et al., The Galileo Solid State Imaging Experiment, *Space Sci. Rev., 60*, 413-455, 1992.

Bevington, P. R., *Data Reduction and Error Analysis for the Physical Sciences*, McGraw-Hill, New York, 1969.

Clarke, J. T., et al., Far-ultraviolet imaging of Jupiter's aurora and the Io "footprint", *Science, 274*, 404-409, 1996.

Cook, A. F. II, A. V. Jones, and D. E. Shemansky, Visible aurora in Jupiter's atmosphere?, *J. Geophys. Res., 86*, 8793-8796, 1981.

Hendrix, A. R., The Galileo Ultraviolet Spectrometer: In-flight calibration and ultraviolet albedos of the moon, Gaspra, Ida, and Europa, Ph.D. thesis, Univ. of Colo., Boulder, 1996.

Hord, C. W., R. A. West, K. E. Simmons, D. L. Coffeen, M. Sato, A. L. Lane, and J. T. Bergstralh, Photometric observations of Jupiter at 2400 angstroms, *Science, 206*, 956-959, 1979.

Hord, C. W., et al., Galileo Ultraviolet Spectrometer Experiment, *Space Sci. Rev., 253*, 1992.

Hord, C. W., et al., Direct observations of Comet Shoemaker-Levy 9 fragment G impact by Galileo UVS, *Geophys. Res. Lett., 22*, 1565-1568, 1995.

James, G. K., J. M. Ajello, and W. R. Pryor, The MUV-visible spectrum of H_2 excited by electron impact, *J. Geophys. Res.*, this issue.

Khakoo, M. A., and S. Trajmar, Electron-impact excitation of the $a\ ^3\Sigma_g^+$, $B\ ^1\Sigma_u^+$, $c\ ^3\Pi_u$, and $C\ ^1\Pi_u$ states of H_2, *Phys. Rev., 34*, 146-156, 1986.

Liu, X., D. E. Shemansky, S. M. Ahmed, M. Ciocca, G. K. James, and J. M. Ajello, Electron impact cross sections of the Lyman and Werner band systems of hydrogen, *Astrophys. J.*, in press, 1998.

Opal, C. B., W. K. Peterson, and E. C. Beaty, Measurements of secondary-electron spectra produced by electron impact ionization of a number of simple gases, *J. Chem. Phys., 55*, 4100-4106, 1971.

Osterbrock, D. E., *Astrophysics of Gaseous Nebulae*, W. H. Freeman, New York, 1974.

Pryor, W. R., and C. W. Hord, A study of photopolarimeter system UV absorption data on Jupiter, Saturn, Uranus, and Neptune - Implications for auroral haze formation, *Icarus, 91*, 161-172, 1991.

Figure 1. Galileo UVS F- and G-channel fields of view illustrated for two typical Jupiter observations near 90° phase angle. The F-channel field of view is smaller and nested inside the G-channel field of view. (a) The observing geometry for the reference reflected solar spectrum obtained on 1996 day 348 06:36-07:36 that was used in our modeling to represent off-axis scattered light. (b) A darkside auroral observation from 1996 day 304 07:38-08:07. These observations were generally done as far on the darkside as possible to minimize off-axis scattered light from Jupiter's dayside.

Figure 2. Viewing geometry for the F- and G-channel fields-of-view during the C3 turn south polar observations of Jupiter on 1996 day 314 05:48-06:01. Galileo was in Jupiter's shadow. The Io torus auroral oval and the more polar reference auroral oval (thought to be the source of the emissions) are shown (J. Clarke, personal communication, 1996). The geometry is shown at (a) the start (05:48), (b) the midpoint (05:54), and (c) near the end (06:00) of the observation.

Figure 3. Total counts in each 4 1/3 s spectrum obtained in the C3 turn south polar observations indicated for (top) the FUV G channel and (bottom) the MUV F channel. Instrument background has not been subtracted.

Figure 4. Summed spectra for the C3 turn south polar observations shown (top) for the FUV G channel and (bottom) for the MUV F channel. The G-channel spectrum, shown as counts per wavelength step, shows H Lyman α (1216 Å) and H_2 band emissions. The F-channel spectrum is very similar to a solar spectrum that has been multiplied by the instrument in-flight calibration [*Hendrix*, 1996]. A substantial instrumental background is also present. To obtain reasonable F-channel signal-to-noise, counts from 10 neighboring wavelength steps have been co-added.

Figure 5. Summed F-channel (MUV) darkside north and south polar spectrum from 90° phase. Three multiple linear regression fits are also shown: (1) a fair fit using just a background-subtracted Jupiter polar dayside spectrum to represent the off-axis light contribution; (2) a better fit using the off-axis contribution and a 14 eV e^- on H_2 laboratory spectrum; and (3) a similar fit using the off-axis contribution and a 19 eV e^- on H_2 laboratory spectrum. To obtain reasonable F-channel signal-to-noise, counts from 10 neighboring wavelength steps have been co-added.

Figure 6. Jupiter darkside polar MUV spectrum from Figure 5 after subtraction of the solar contribution, leaving just the auroral component. In the upper panel, the solar part of regression (2) just described has been subtracted and is compared to the 14 eV e^- on H_2 laboratory spectrum [*James et al.*, this issue] and in the lower panel, the solar part of regression (3) just described has been subtracted and is compared to the 19 eV e^- on H_2 laboratory spectrum [*James et al.*, this issue]. The fit in the upper panel is slightly superior. Again, counts from 10 neighboring wavelength steps have been co-added. The 1-σ statistical uncertainty in the 10 grating step wide bin is shown.

H_2 laboratory spectrum, (3) an identical fit using the off-axis contribution and a 19 eV e^- on H_2 laboratory spectrum. To obtain reasonable F-channel signal-to-noise, counts from 40 neighboring wavelength steps have been co-added.

Figure 8. The Jupiter darkside FUV summed auroral spectrum obtained simultaneously with the dimmer MUV auroral spectrum in Figure 6, compared to the UVS laboratory spectrum of 100 eV e^- on H_2. Short-wavelength differences are attributed to CH_4 absorption in Jupiter's atmosphere and to electron energy effects. Note the absence of reflected solar contributions to the FUV spectrum.

Table 2. Model emission ratios from different electron distributions compared to UVS data ratio.

	Photon Flux Ratio	
	FUV (1230-1650 Å)/ MUV (1616.5-3227.9Å)	FUV (1500-1650Å)/ MUV (1616.5-3227.9Å)
Galileo UVS polar data	8.1	3.9
Opal distribution	2.8	1.3
27 eV distribution	7.5	3.4
50 eV distribution	16.9	7.5
100 eV distribution	43.7	19.5

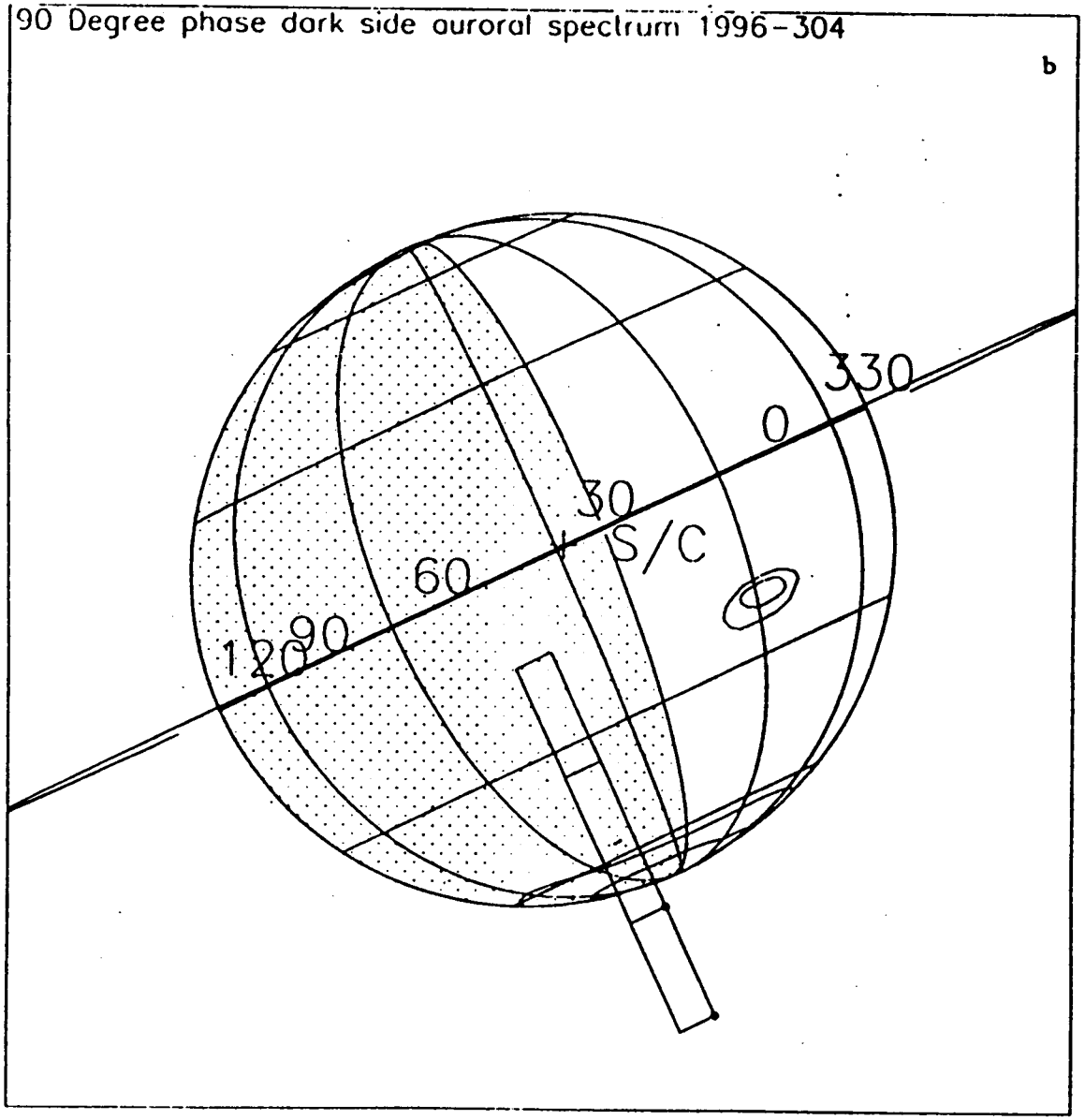
90 Degree phase dark side auroral spectrum 1996-304
b
330
0
30
S/C
60
90
120

F15

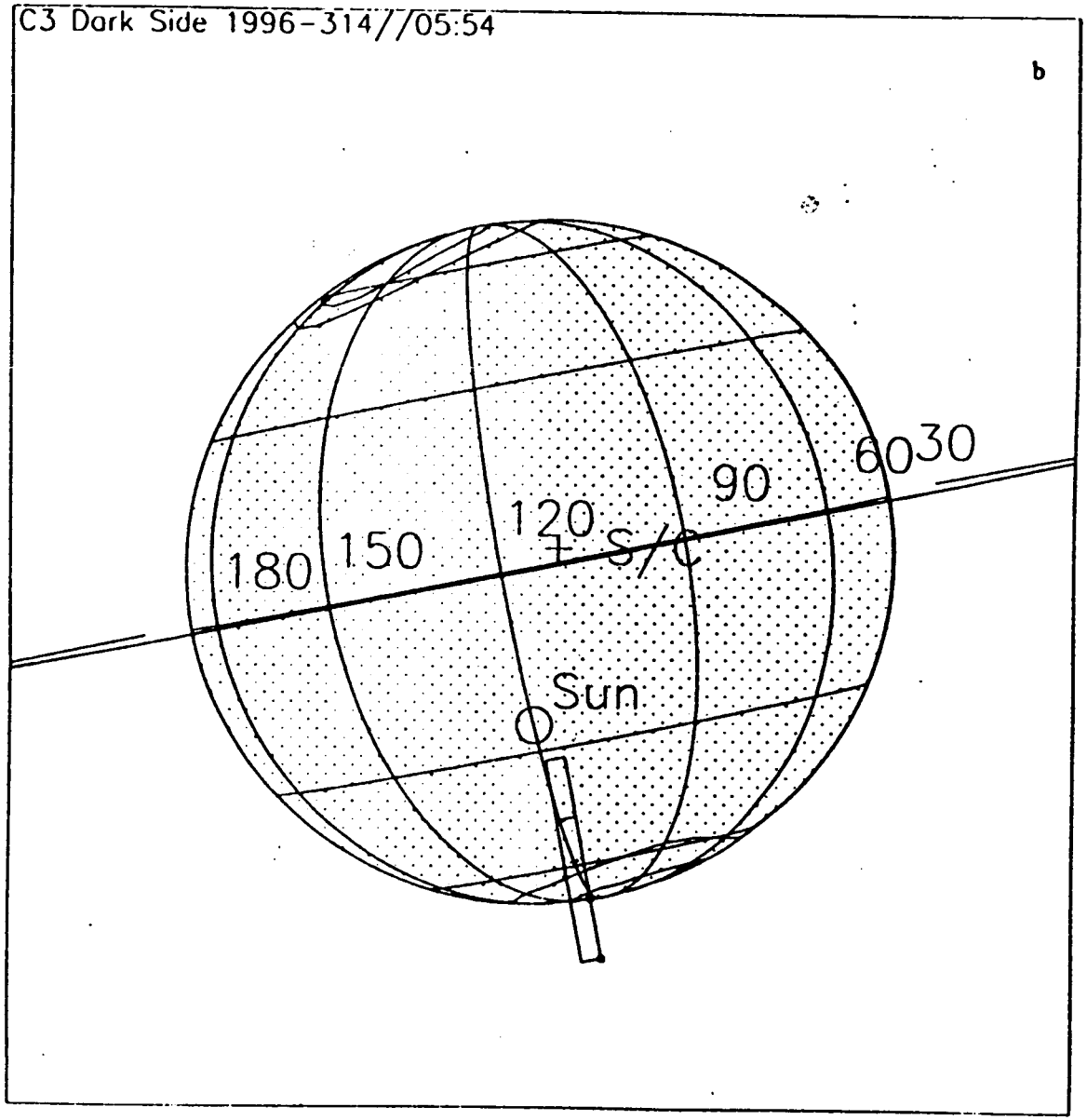
C3 Dark Side 1996-314//05:54
b
180
150
120
90
60
30
S/C
Sun

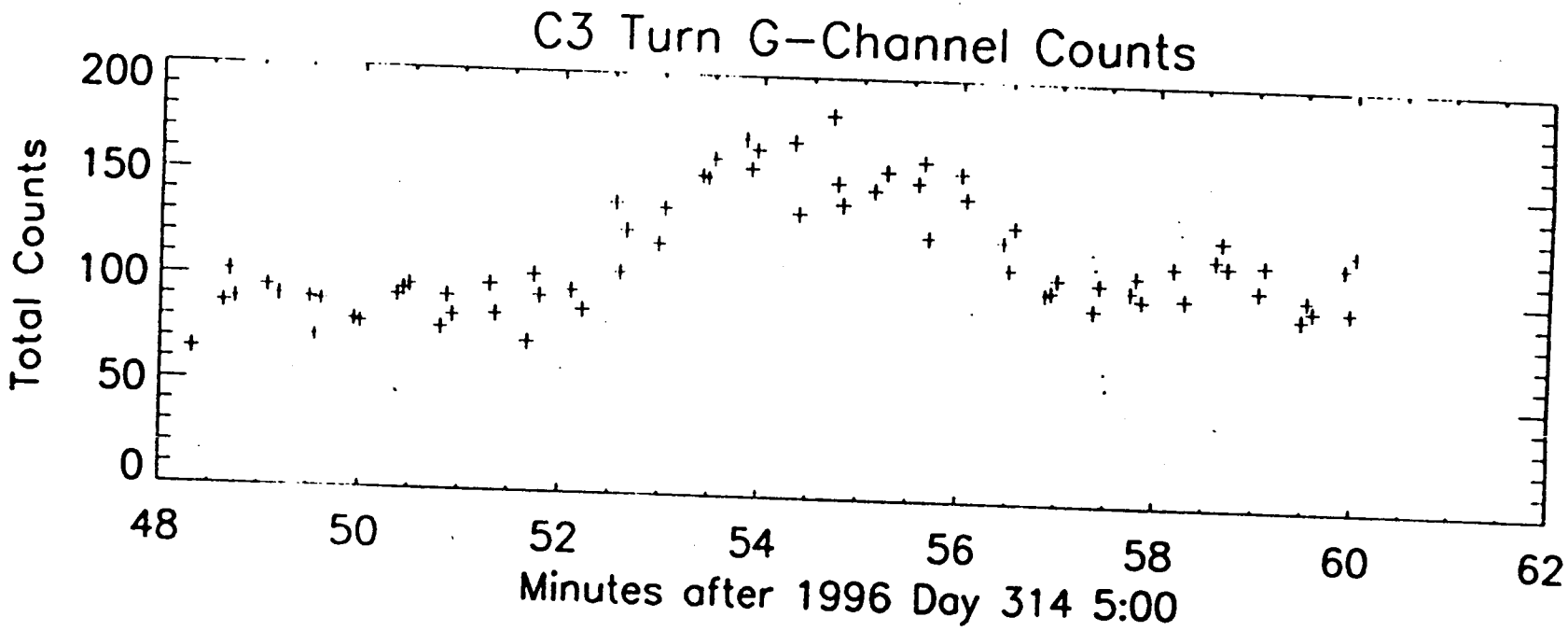
C3 Turn G–Channel Counts
Total Counts
200
150
100
50
0
48
50
52
54
56
58
60
62
Minutes after 1996 Day 314 5:00

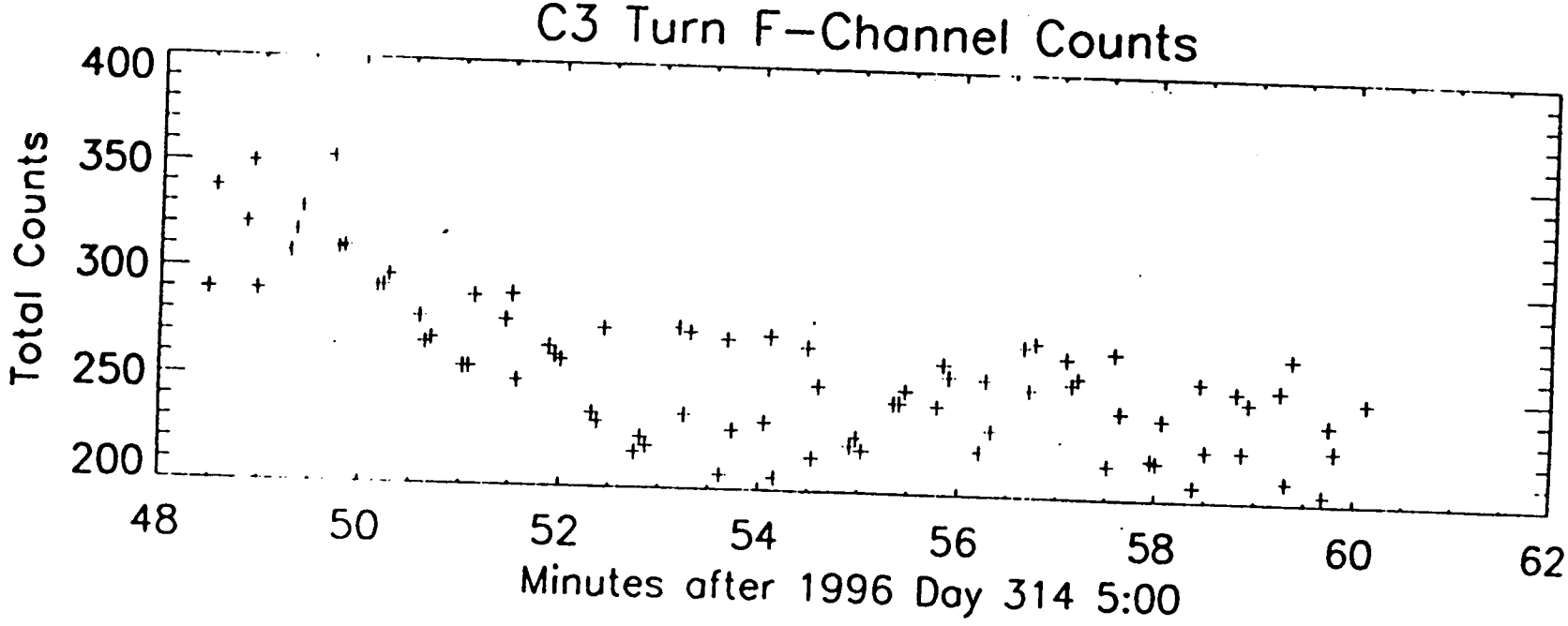
C3 Turn F–Channel Counts
Total Counts
400
350
300
250
200
48
50
52
54
56
58
60
62
Minutes after 1996 Day 314 5:00

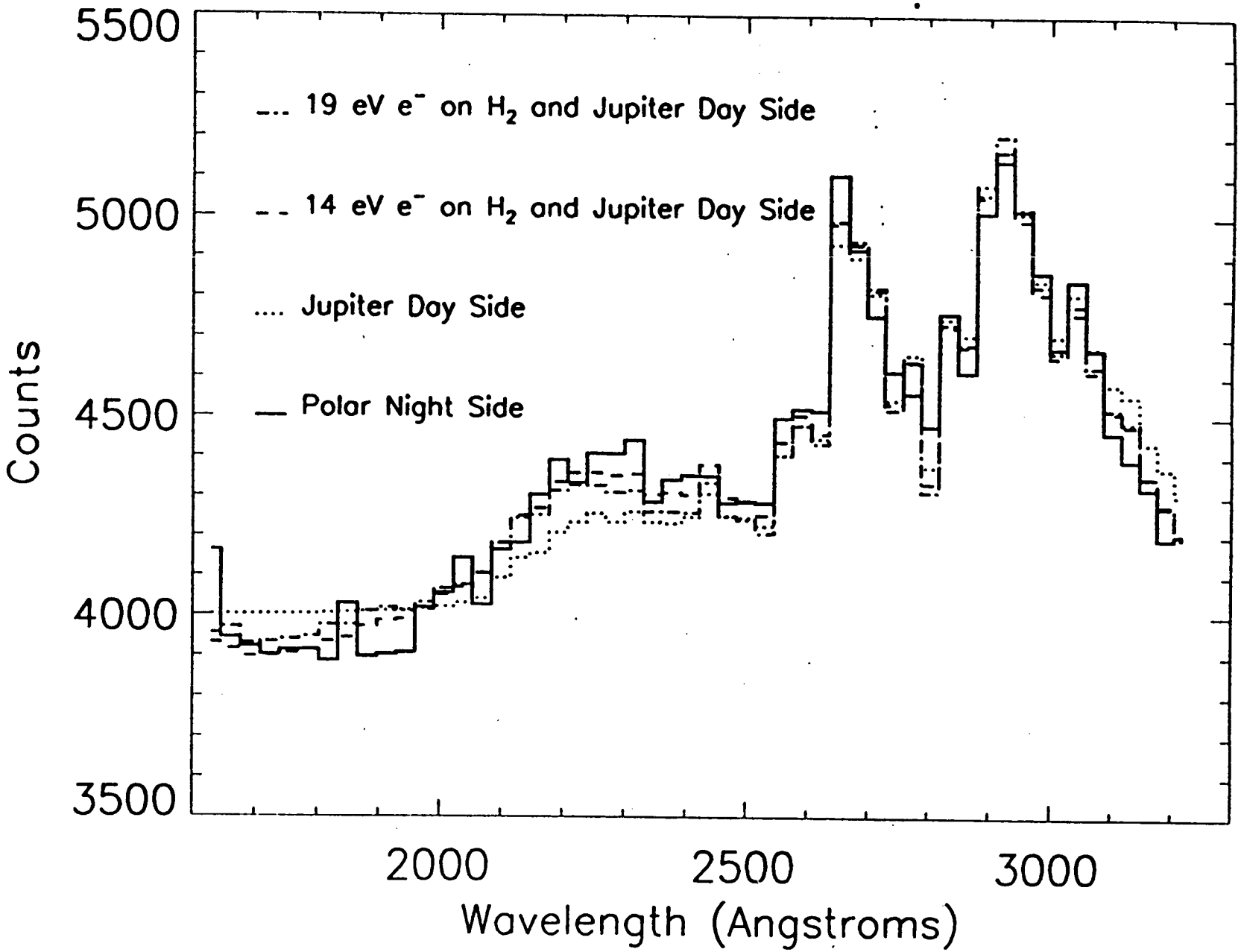
5500
5000
4500
4000
3500
Counts
--- 19 eV e⁻ on H₂ and Jupiter Day Side
- - 14 eV e⁻ on H₂ and Jupiter Day Side
.... Jupiter Day Side
— Polar Night Side
2000
2500
3000
Wavelength (Angstroms)

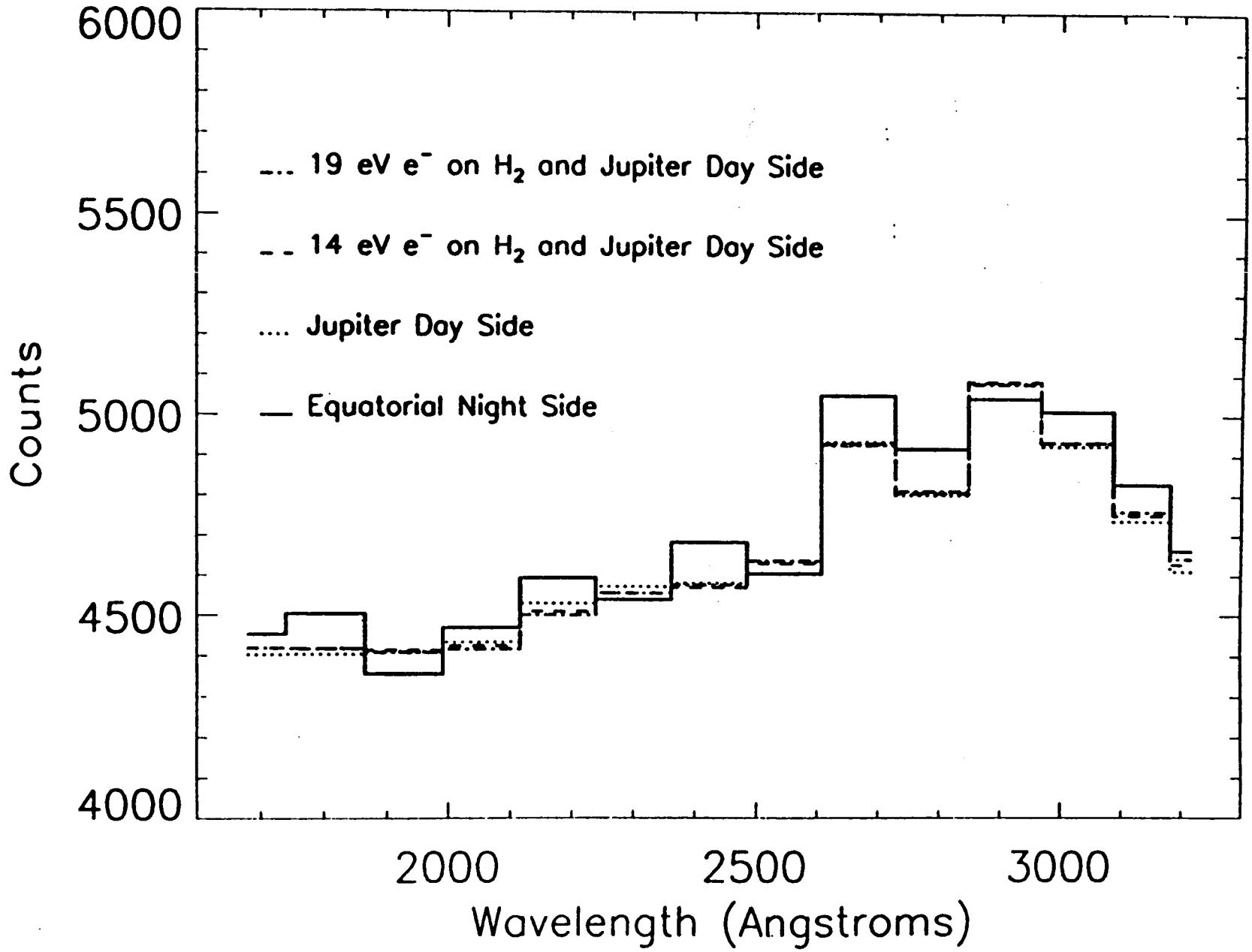
6000
5500
5000
4500
4000
Counts
--- 19 eV e⁻ on H₂ and Jupiter Day Side
-- 14 eV e⁻ on H₂ and Jupiter Day Side
.... Jupiter Day Side
— Equatorial Night Side
2000
2500
3000
Wavelength (Angstroms)